

This discussion paper is/has been under review for the journal Atmospheric Chemistry and Physics (ACP). Please refer to the corresponding final paper in ACP if available.

Size distributions of mineral aerosols and dust emission flux

X. Li and H. S. Zhang

Size distributions of mineral aerosols and dust emission flux observed over Horqin Sandy Land area in northern China

X. Li and H. S. Zhang

Laboratory for Climate and Ocean-Atmosphere Studies, Department of Atmospheric and Oceanic Sciences, School of Physics, Peking University, China

Received: 22 November 2012 – Accepted: 9 January 2013 – Published: 24 January 2013

Correspondence to: H. S. Zhang (hsdq@pku.edu.cn)

Published by Copernicus Publications on behalf of the European Geosciences Union.

Title Page

Abstract

Introduction

Conclusions

References

Tables

Figures

⏪

⏩

◀

▶

Back

Close

Full Screen / Esc

Printer-friendly Version

Interactive Discussion



Abstract

Size distribution of mineral aerosols is of primary importance in determining their residence time in atmosphere, transport patterns, removal mechanisms as well as their effects on climate and human health. This study aims to obtain dust particle size distribution and size-resolved dust emission flux under different weather conditions over a sandy land area in northern China (Horqin Sandy Land, Inner Mongolia), using the observational data from Horqin sandstorm monitoring station in the spring of 2010 and 2012. Dust (PM_{20}) mass concentration was measured by a 10-stage quartz crystal microbalance (QCM) cascade impactor. The statistical results indicate that finer dust particles ($r \leq 1.0 \mu\text{m}$) take a large proportion of all PM_{20} concentration under clear-day conditions, while coarser dust particles ($r \geq 2.5 \mu\text{m}$) concentration increased under dust-day conditions, with the peak occurring between 4–7 μm . The dust particle size distributions during the pre-dust-emission and dust-emission periods of a dust event on 7 April 2012 have similar features to the statistical results. During the dust event, the magnitude of dust emission flux of all sizes increased about one or two orders ($0.1\text{--}10 \mu\text{g m}^{-2} \text{s}^{-1}$) as u_* increase from 0.54 to 1.29 m s^{-1} . The maximum total F value was about $43.0 \mu\text{g m}^{-2} \text{s}^{-1}$ and the maximum size-resolved $F(D_{di})$ is $12.3 \mu\text{g m}^{-2} \text{s}^{-1}$ in 0.3–0.45 μm size bin when u_* is 1.29 m s^{-1} . Dust advection has effects on airborne dust size distribution, making the proportion of dust particles of different sizes more uniform, as observed in a non-local dust event on 19 April 2012.

1 Introduction

Mineral aerosols generated by wind erosion from many arid and semi-arid areas in the world play an important role in many physics, chemical and biogeological processes of the Earth system (Shao et al., 2011). They are particularly vital for the climate system, as they influence the atmospheric radiation balance directly through scattering and absorbing various radiation components (Sokolik and Golitsyn, 1993; Tegen et al.,

ACPD

13, 2671–2693, 2013

Size distributions of mineral aerosols and dust emission flux

X. Li and H. S. Zhang

Title Page

Abstract

Introduction

Conclusions

References

Tables

Figures

⏪

⏩

◀

▶

Back

Close

Full Screen / Esc

Printer-friendly Version

Interactive Discussion



1996), and indirectly through modifying the optical properties and lifetime of clouds (Mahowald and Kiehl, 2003; Andreae and Rosenfeld, 2008). Among a range of parameters that are used to describe aerosol properties, aerosol size distribution is of great importance for the estimation and prediction of dust emission, transport and deposition processes as well as their effects on climate and human health (Alfaro et al., 1998). Since mineral aerosols of different sizes have profoundly different optical, aerodynamic and mineralogical characteristics, it is desirable to obtain the dust emission flux for different particle size range (Shao, 2008). However, size distribution of suspending dust particles always changes with time during dust events. It greatly depends on wind conditions, local soil properties and land-surface characteristics (Westphal et al., 1987; Gomes et al., 1990; Alfaro et al., 1998) and is more or less influenced by dust particles transported from other regions (Zhang et al., 1998; Maring et al., 2003). Additionally, it can probably be affected by the sand supply limitation during dust generations (Lopez, 1998; Gillette and Ono, 2008).

Many field and wind tunnel experiments have been conducted to study the size distributions of mineral aerosols under different wind and soil conditions. For example, Gillette et al. (1972) measured the aerosol ($0.3 \leq r \leq 6 \mu\text{m}$) size distributions at 1.5 and 6 m height in a field in rural Nebraska, and the measured size distribution had a power law for $0.3 \leq r \leq 1 \mu\text{m}$, $dN/d(\log r) \propto r^{-2}$, and a flatter curve for $1 \leq r \leq 6 \mu\text{m}$ at both heights during dust emission periods. Gomes et al. (1990) observed a second mass peak of submicron particles for Saharan aerosols ($0.1 \leq r \leq 20 \mu\text{m}$) under strong wind-erosion conditions, which is consistent with the theory that the sandblasting process (saltation) is the major mechanism for dust emission (Gillette and Walker, 1977). Alfaro et al. (1997, 1998) carried out a series of wind tunnel experiments to study particle size distribution under different wind conditions. They used pure quartz sand particles to bombard various surfaces made of kaolin clay, nature loamy and sandy soils. Their results indicated that for relatively small friction velocity u_{*} , the size distribution of the airborne dust was close to that of the original erodible fractions, however, for higher u_{*} , the size spectrum showed a new peak around a smaller diameter. These previous

Size distributions of mineral aerosols and dust emission flux

X. Li and H. S. Zhang

[Title Page](#)[Abstract](#)[Introduction](#)[Conclusions](#)[References](#)[Tables](#)[Figures](#)[◀](#)[▶](#)[◀](#)[▶](#)[Back](#)[Close](#)[Full Screen / Esc](#)[Printer-friendly Version](#)[Interactive Discussion](#)

studies contribute to the development of size-dependent dust emission schemes in dust emission models (Lu and Shao, 1999; Shao, 2004) and lay a solid foundation for the precise modeling of dust emission, transport and deposition.

Asian dust events are a typical example of mineral-aerosol storms that frequently originates in the sand desert, Gobi desert, Loess plateau, and the mixed barren soil in northern China and Mongolia all year round when meteorological and soil surface conditions are satisfied for the dust rise (Park et al., 2010; Li and Zhang, 2012). Many researchers have studied the changes of dust particle size distributions during long-range transport of Asian dust (e.g. Maring et al., 2003; Park and Kim, 2006; Kobayashi et al., 2007). However, to the best of my knowledge, studies related to the characteristics of size-resolved dust emission flux during Asian dust events over their source regions are relatively rare due to the lack of long-term field measurements of dust concentration in different sizes.

In the present study, observational data obtained from a sandstorm monitoring station in Horqin Sandy Land area in northern China in the spring of both 2010 and 2012 were used to investigate the characteristics of dust particle ($0.1 \leq r \leq 20 \mu\text{m}$) size distribution under different weather conditions and to analyze the variation of size-resolved dust emission flux under different wind conditions. The detailed description of the observational site and data is given in Sect. 2. The characteristics of size distribution of dust concentration and dust emission flux under different weather conditions are demonstrated in Sect. 3. Conclusions are eventually drawn in Sect. 4.

2 Data and methods

2.1 Experiment site

The observational data were obtained from a sandstorm monitoring station ($42^{\circ}27' \text{N}$, $120^{\circ}42' \text{E}$) in the eastern edge of largest sandy land area in China, the Horqin Sandy Land, which is about 500 km to the northeast of Beijing, the capital of China (Fig. 1a).

Size distributions of mineral aerosols and dust emission flux

X. Li and H. S. Zhang

Title Page

Abstract

Introduction

Conclusions

References

Tables

Figures

⏪

⏩

◀

▶

Back

Close

Full Screen / Esc

Printer-friendly Version

Interactive Discussion



The surrounding landscape of the station is featured by gently undulating, shifting and semi-shifting dunes as well as fixed dunes with largely low, open shrub vegetation (Zhao et al., 2007), as shown in Fig. 1b.

A 20-m triangular lattice mast equipped with many meteorological instruments to measure 4 levels (2, 4, 16, and 20 m) of wind speed (A100LM, Vector Instruments) and air temperature and humidity (HMP45C, Vaisala, Inc.), wind direction (W200P, Vector Instruments) at 20 m height, short radiation (LI200X, LI-COR) and net radiation (Nr-Lite, Kipp & Zonen) at 2 m height, 3 depths (5, 10 and 20 cm) of soil temperature (107, Campbell Scientific, Inc.) and soil water content (CS616, Campbell Scientific, Inc.), as well as the turbulence of wind and temperature (CSAT3, Campbell Scientific, Inc.) at 8 m height. In addition, dust (PM₁₀) concentrations were measured by beta gauge (FH62C14, Thermo Scientific) at 3 m and 18 m heights to calculate dust emission flux. The saltation activities of sand particles ($r > 50 \mu\text{m}$) can be observed by a wind eroding mass sensor (H11B Sensit Sensor) at the height of 0.75 m above the surface.

All the conventional meteorological and dust parameters were recorded automatically and continuously with a sample interval of 10 min. The 10-min data were dealt with a 30-min moving average. The turbulence measurements were recorded with a frequency response of 10 Hz and were also processed to be the 30-min data.

2.2 Spectral dust mass concentration measurements

Dust (PM₂₀) mass concentration were measured by a 10-stage quartz crystal microbalance (QCM) cascade impactor (PC-2HX, California Measurements, Inc.) at 3 m height. The size cutoff diameters for each stage are 10, 7, 4, 2.5, 1.4, 0.7, 0.45, 0.3, 0.2 and 0.1 μm . As particle-laden air passes through the stages progressively, smaller and smaller particles are collected as the airflow moves down towards stage 10. The collected particles on the QCM crystals cause the change in the frequency signal outputs. As soon as the frequency change (dF) between the sensing crystal and reference crystal in any one of the stages reaches a preset level, the software in the control unit

Size distributions of mineral aerosols and dust emission flux

X. Li and H. S. Zhang

Title Page

Abstract

Introduction

Conclusions

References

Tables

Figures

◀

▶

◀

▶

Back

Close

Full Screen / Esc

Printer-friendly Version

Interactive Discussion



terminates the sampling by sending a signal to shut off the inlet valve. The value of dF was set to 40 Hz in April 2010, 60 Hz in May 2010 and 70 Hz from March to May 2012.

The observed dust mass concentrations by QCM cascade impactor are required to be calibrated with the observations from beta gauge at the same 3 m height, because the QCM measurements usually have underestimations under high concentration conditions ($\sim 1000 \mu\text{g m}^{-3}$). However, the proportion of dust concentration among various stages are reliable, hence the PM_{10} concentration values observed by QCM cascade impactor can be calibrated with observations by beta gauge, and then dust concentration of all sizes can be reversely calculated by multiplying their ratios to the PM_{10} concentration. Figure 3 shows the scatter plot of PM_{10} concentration measured by the QCM cascade impactor against that from beta gauge at the same time. The QCM observations were mostly lower than the beta gauge values. The optimal fitting relationships between them at different dF values are also shown in Fig. 2.

2.3 Methods

The data on wind speed and air temperature profile were used to calculate friction velocity, u_* , based on Monin–Obukhov similarity theory (Garratt, 1992; Zhu et al., 2008):

$$u_* = \kappa U(z) \left[\ln \left(\frac{z}{z_0} \right) - \psi_m \left(\frac{z}{L} \right) + \psi_m \left(\frac{z_0}{L} \right) \right]^{-1}, \quad (1)$$

where κ is von Karman's constant, here taken as 0.4; $U(z)$ is the mean wind speed at the 4 m and 16 m heights, $z = 10$ m; z_0 is the roughness length; L is the Obukhov length; and Ψ_m is the momentum stability function.

Dust emission flux F can be computed using dust concentration gradient measurements based on the assumption that the particles with aerodynamic diameters $< 10 \mu\text{m}$ were light enough to follow air movements perfectly (Gillette, 1972; Zhang et al., 2007; Sow et al., 2009; Li and Zhang, 2012).

Size distributions of mineral aerosols and dust emission flux

X. Li and H. S. Zhang

Title Page

Abstract

Introduction

Conclusions

References

Tables

Figures

◀

▶

◀

▶

Back

Close

Full Screen / Esc

Printer-friendly Version

Interactive Discussion



$$F = \kappa u_* (C_1 - C_2) \left[\ln \left(\frac{z_2}{z_1} \right) - \psi_m \left(\frac{z_2}{L} \right) + \psi_m \left(\frac{z_1}{L} \right) \right]^{-1}, \quad (2)$$

where C_1 and C_2 are the dust mass concentration at $z_1 = 3$ m and $z_2 = 18$ m height, respectively. Other variables are the same as in Eq. (1).

Assuming the airborne particle size distribution $p(d)$ is the same at 3 and 18 m height, the dust emission flux in the i -th size bin $F(D_{di})$ can be calculated by the following equation:

$$F(D_{di}) = \int F \cdot p(d) \delta d, \quad (3)$$

where F is dust emission flux obtained from Eq. (2).

3 Results

3.1 Statistical characteristics of airborne dust particle size distribution

A total of 29 samples under clear-day conditions and 16 samples under dust-day conditions measured by QCM cascade impactor in the spring (March, April and May) of 2010 and 2012 were selected through strict data quality control. A dust sample means that PM_{10} concentration measured by beta gauge at 3 m height is larger than $150 \mu\text{g m}^{-3}$ and wind speed at 4 m height is larger than 6 m s^{-1} . As shown in Fig. 3, there are two peaks in the mean size distribution of airborne dust particles under clear-day and dust-day conditions – one between 0.30 – $0.45 \mu\text{m}$ and the other between 4.0 – $7.0 \mu\text{m}$. The size distributional curves look similar to each other, but the difference is that finer dust particles ($r \leq 1.0 \mu\text{m}$) take a large proportion of all dust concentration under clear-day conditions, while coarser dust particles ($r \geq 2.5 \mu\text{m}$) concentration increases under dust-day conditions.

Size distributions of mineral aerosols and dust emission flux

X. Li and H. S. Zhang

Title Page

Abstract

Introduction

Conclusions

References

Tables

Figures

◀

▶

◀

▶

Back

Close

Full Screen / Esc

Printer-friendly Version

Interactive Discussion



3.2 Size distribution of dust concentration and dust emission flux for dust events

Table 1 shows the period of sampling, the maximum concentration reached at 3 m height and the meteorological parameters for all observed dust events in April 2012 according to the relative definition in Li and Zhang (2011). Among these dust events, the one that occurred on 7 April was observed by us as we visited the station. We will take it as an example for the following analysis.

3.2.1 Temporal variations in some meteorological and dust parameters during the dust event on 7 April 2012

Figure 4a shows the temporal variations of dust concentration measured by beta gauges at 3 and 18 m height and wind direction at 20 m height on 7 April 2012. The values of dust concentration at the two levels were mostly below $100.0 \mu\text{g m}^{-3}$ before 08:00 (LT, here after), and then gradually increased with time as wind speed increased (Fig. 5b). There were two peaks of dust concentration at 3 m height, one of $322.8 \mu\text{g m}^{-3}$ at 16:00 and the other of $350.5 \mu\text{g m}^{-3}$ at 22:40. Southern flows ($\sim 180^\circ$) dominated during most of the day, while northern winds ($\sim 340^\circ$) suddenly prevailed after 21:00 at night.

The temporal variations of wind speed at 4 m height and Sensit Sensor response numbers on 7 April are shown in Fig. 4b. It should be noted that the saltation intensity of sand particles is sensitive to observation height: the higher the observation height, the weaker the saltation behavior was observed. Although the observation height is relatively higher in this study than the lowest observation height in most previous studies, e.g. the Sensit Sensors were equipped at heights of 5, 10, 20, 50 and 100 cm in Gillette et al. (2008), the response number is still able to reflect the change trends of saltation process. It can be found that saltation intensity became stronger as wind speed increased from 12:00 to 18:00 LT. The maximum response number was 17 at 15:10 along with the maximum wind speed of 9.7 m s^{-1} at the same time.

Size distributions of mineral aerosols and dust emission flux

X. Li and H. S. Zhang

Title Page

Abstract

Introduction

Conclusions

References

Tables

Figures

◀

▶

◀

▶

Back

Close

Full Screen / Esc

Printer-friendly Version

Interactive Discussion



The variation of friction velocity u_* highly follow closely that of wind speed (Fig. 4c). It can be found that the high dust emission flux F usually corresponded to the periods of high saltation intensity (Fig. 5c). This is in agreement with the theory that saltation process is the major mechanism for dust emission. The maximum F value was about 43.0 $\mu\text{g m}^{-2} \text{s}^{-1}$ at 16:10 during the dust storm event.

3.2.2 Size-resolved dust concentration and dust emission flux during the dust event on 7 April 2012

Figure 5 shows the ratio of dust concentration in each size bin c (D_{di}) to the PM_{10} concentration c that was measured by QCM cascade impactor several times during the dust event on 7 April 2012. As u_* was relatively small ($< 0.7 \text{ m s}^{-1}$) before the breakout of dust event, the size peaks were shown in $0.2 \leq r \leq 0.45 \mu\text{m}$ and next in $4 \leq r \leq 7 \mu\text{m}$. Most of the airborne dust particles were less than $1 \mu\text{m}$ in size; however, hardly any coarser particles ($r \geq 7 \mu\text{m}$) were detected (Fig. 5a). When the sand storm broke out and u_* increased to 1.2 m s^{-1} , a small amount of coarser particles were measured. Dust particles in $4\text{--}7 \mu\text{m}$ size took up the largest amount of the total PM_{20} concentration, increasing from 10% to 40%, and exceeded the concentration in $0.2\text{--}0.45 \mu\text{m}$ size (Fig. 5b).

The size-resolved dust emission flux distribution of various samples are displayed in Fig. 6. During this dust event, the magnitude of dust emission flux in various sizes increased about one or two orders ($0.1\text{--}10 \mu\text{g m}^{-2} \text{s}^{-1}$) as u_* increased from 0.54 to 1.29 m s^{-1} . The maximum of dust emission flux in $0.3\text{--}0.45 \mu\text{m}$ size bin is $12.3 \mu\text{g m}^{-2} \text{s}^{-1}$ when u_* is 1.29 m s^{-1} .

3.3 Effects of dust advection on airborne dust particle size distribution

It is interesting to notice a different feature in the size-resolved dust emission flux distribution during the dust event on 19 April 2012. As shown in Fig. 8, finer particles ($r \leq 1.0 \mu\text{m}$) still contributed most to the total airborne dust particles; however, the

Size distributions of mineral aerosols and dust emission flux

X. Li and H. S. Zhang

Title Page

Abstract

Introduction

Conclusions

References

Tables

Figures

◀

▶

◀

▶

Back

Close

Full Screen / Esc

Printer-friendly Version

Interactive Discussion



proportion of dusts in the 0.7–1.4 μm size bin considerably increased and dusts in the 4–7 μm size bin relatively decreased. By comparison with the particle size distribution during the dust event on 7 April 2012, as shown in Fig. 6, the proportion of airborne dust particles of different sizes – especially coarser particles – looks more uniform during the dust event on 19 April 2012.

The more uniform proportion in the particle size distribution on 19 April 2012 is probably relate to dust advection. The F values can be used to distinguish the local dust event in which the high dust concentration is mainly due to local dust emission and the non-local dust event in which the high dust concentration is influenced by dust advection (Li and Zhang, 2012). The positive F values mean dust particles are transported from the low levels to the high and identify the local dust event, while the negative F values represent the non-local dust event. According to the definition, the negative F values occurred in the periods of 12:00–14:00 and 17:00–20:00 during the dust event on 19 April 2012 (Fig. 8b), and dust advection influenced the dust particle size distribution. Through mixing with dusts from upstream regions, it is easy to understand why the difference among the proportion of course particles reduced during the non-local dust event on 19 April 2012.

4 Conclusions

In this study, observational data that were obtained from the Naiman station located in Horqin Sandy Land area of northern China in the spring of both 2010 and 2012 were used to analyze the characteristics of dust particle size distributions and the variations of size-resolved dust emission flux during different dust events under various weather conditions. Dust (PM_{20}) mass concentration was measured by a 10-stage quartz crystal microbalance (QCM) cascade impactor.

The statistical results indicate that finer dust particles ($r \leq 1.0 \mu\text{m}$) have a large proportion of all PM_{20} concentration under clear-day conditions, and coarser dust particles

Size distributions of mineral aerosols and dust emission flux

X. Li and H. S. Zhang

Title Page

Abstract

Introduction

Conclusions

References

Tables

Figures

◀

▶

◀

▶

Back

Close

Full Screen / Esc

Printer-friendly Version

Interactive Discussion



($r \geq 2.5 \mu\text{m}$) increase under dust-day conditions and their sizes mostly focused between 4–7 μm .

The case analysis for the local dust event on 7 April 2012 shows that the airborne dust particle size distribution has a first peak in the 0.2–0.3 μm size bin and a second peak in the 4–7 μm size bin in the pre-dust-emission period with u_* close to 0.6 m s^{-1} . However, the first peak changed to be the 4–7 μm size bin and the proportion of finer dusts ($r \leq 1 \mu\text{m}$) reduced during the dust-emission period with u_* larger than 1.2 m s^{-1} . Dust particles with diameters between 1.4–4.0 μm and 10–20 μm took up only a small proportion. The magnitude of dust emission flux of all sizes increased about one or two orders ($0.1\text{--}10 \mu\text{g m}^{-2} \text{ s}^{-1}$) as u_* increased from 0.54 to 1.29 m s^{-1} . The maximum F value for PM_{10} was about $43.0 \mu\text{g m}^{-2} \text{ s}^{-1}$ and the maximum size-resolved $F(D_{di})$ is $12.3 \mu\text{g m}^{-2} \text{ s}^{-1}$ in 0.3–0.45 μm size bin when u_* is 1.29 m s^{-1} .

Based on the case analysis for the non-local dust event on 19 April 2012, it was found that dust advection influenced the airborne dust size distribution. Dust advection can be identified with negative F values. It made the proportion of dust particles of different sizes, especially coarser dusts tend to be more uniform, when local dust particles were mixed with non-local dusts transported from upstream regions.

Acknowledgements. This work was jointly funded by the National Natural Science Foundation of China (41075005), National Program on Key Basic Research Project of China (973) (2010CB428501), R&D Special Fund for Public Welfare Industry (meteorology) by Ministry of Finance and Ministry of Science and Technology (GYHY201006014), as well as RFDP (20110001130010).

References

Alfaro, S. C., Gaudichet, A., Gomes, L., and Maillé, M.: Modeling the size distribution of a soil aerosol produced by sandblasting, *J. Geophys. Res.*, 102, 11239–11249, doi:10.1029/97JD00403, 1997.

Size distributions of mineral aerosols and dust emission flux

X. Li and H. S. Zhang

Title Page

Abstract

Introduction

Conclusions

References

Tables

Figures

◀

▶

◀

▶

Back

Close

Full Screen / Esc

Printer-friendly Version

Interactive Discussion



Alfaro, S. C., Gaudichet, A., Gomes, L., and Maillé, M.: Mineral aerosol production by wind erosion: Aerosol particle sizes and binding energies, *Geophys. Res. Lett.*, 25, 991–994, doi:10.1029/98GL00502, 1998.

Andreae, M. O. and Rosenfeld, D.: Aerosol-cloud-precipitation interactions, Pt 1, The nature and sources of cloud-active aerosols, *Earth-Sci. Rev.*, 89, 13–41, 2008.

Garratt, J. R.: The atmospheric boundary layer, Cambridge, Cambridge University Press, 52–53, 1992.

Gillette, D. A. and Ono, D.: Expressing sand supply limitation using a modified Owen saltation equation, *Earth Surf. Proc. Land.*, 33, 1806–1813, 2008.

Gillette D. A. and Walker T.: Characteristics of airborne particles produced by wind erosion of sandy soil, high plains of west Texas, *Soil Science*, 123, 97–110, 1977.

Gillette, D. A., Blifford, I. H., and Fenster, C. R.: Measurements of aerosol size distributions and vertical fluxes of aerosols on land subject to wind erosion, *J. Appl. Meteorol.*, 11, 977–987, 1972.

Gomes, L., Bergametti, G., Coudé-Gaussen, G., and Rognon, P.: Submicron desert dusts, A sandblasting process, *J. Geophys. Res.*, 95, 13927–13935, doi:10.1029/JD095iD09p13927, 1990.

Kobayashi, H., Arao, K., Murayama, T., Iokibe, K., Koga, R., and Shiobara, M.: High-resolution measurement of size distributions of Asian Dust using a Coulter multisizer, *J. Atmos. Oceanic Technol.*, 24, 194–205, 2007.

Li, X. and Zhang, H. S.: Research on threshold friction velocities during dust events over the Gobi Desert in northwest China, *J. Geophys. Res.*, 116, D20210, doi:10.1029/2010JD015572, 2011.

Li, X. and Zhang, H. S.: Temporal variations in dust concentration and dust emission observed over Horqin Sandy Land area from December 2010 to November 2011, *Atmos. Environ.*, 61, 56–65, 2012.

Lopez, M.: Wind erosion in agricultural soils: an example of limited supply of particles available for erosion, *Catena*, 33, 17–28, 1998.

Lu, H. and Shao, Y.: A new model for dust emission by saltation bombardment, *J. Geophys. Res.*, 104, 16827–16842, doi:10.1029/1999JD900169, 1999.

Mahowald, N. M. and Kiehl, L. M.: Mineral aerosol and cloud interactions, *Geophys. Res. Lett.*, 30, 1475, doi:10.1029/2002GL016762, 2003.

Size distributions of mineral aerosols and dust emission flux

X. Li and H. S. Zhang

Title Page

Abstract

Introduction

Conclusions

References

Tables

Figures

◀

▶

◀

▶

Back

Close

Full Screen / Esc

Printer-friendly Version

Interactive Discussion



Size distributions of mineral aerosols and dust emission flux

X. Li and H. S. Zhang

[Title Page](#)[Abstract](#)[Introduction](#)[Conclusions](#)[References](#)[Tables](#)[Figures](#)[◀](#)[▶](#)[◀](#)[▶](#)[Back](#)[Close](#)[Full Screen / Esc](#)[Printer-friendly Version](#)[Interactive Discussion](#)

- Maring, H., Savoie, D. L., Izaguirre, M. A., Custals, L., and Reid, J. S.: Mineral dust aerosol size distribution change during atmospheric transport, *J. Geophys. Res.*, 108, 8592, doi:10.1029/2002JD002536, 2003.
- Park, S.-U. and Kim, J.-W.: Aerosol size distributions observed at the Seoul National University campus in Korea during the Asian dust and non-Asian dust periods, *Atmos. Environ.*, 40, 1722–1730, 2006.
- Park, S.-U., Park, M.-S., and Chun, Y.: Asian dust events observed by a 20-m monitoring tower in Mongolia during 2009, *Atmos. Environ.*, 44, 4964–4972, 2010.
- Shao, Y.: Simplification of a dust emission scheme and comparison with data, *J. Geophys. Res.*, 109, D10202, doi:10.1029/2003JD004372, 2004.
- Shao, Y.: Physics and modelling of wind erosion, *Atmospheric and Oceanographic Sciences Library*, Vol. 37, Kluwer Academic Publishing, Dordrecht, 2008.
- Shao, Y., Ishizuka, M., Mikami, M., and Leys, J. F.: Parameterization of size-resolved dust emission and validation with measurements, *J. Geophys. Res.*, 116, D08203, doi:10.1029/2010JD014527, 2011.
- Sokolik, I. and Golitsyn, G.: Investigation of optical and radiative properties of atmospheric dust aerosols, *Atmos. Environ.*, Pt A, General Topics, 27, 2509–2517, 1993.
- Sow, M., Alfaro, S. C., Rajot, J. L., and Marticorena, B.: Size resolved dust emission fluxes measured in Niger during 3 dust storms of the AMMA experiment, *Atmos. Chem. Phys.*, 9, 3881–3891, doi:10.5194/acp-9-3881-2009, 2009.
- Tegen, I., Lacis, A. A., and Fung, I.: The influence on climate forcing of mineral aerosols from disturbed soils, *Nature*, 380, 419–422, 1996.
- Westphal, D. L., Toon, O. B., and Carlson, T. N.: A two-dimensional numerical investigation of the dynamics and microphysics of Saharan dust storms, *J. Geophys. Res.*, 92, 3027–3049, doi:10.1029/JD092iD03p03027, 1987.
- Westphal, D. L., Toon, O. B., and Carlson, T. N.: A case study of mobilization and transport of Saharan dust, *J. Atmos. Sci.*, 45, 2145–2175, 1988.
- Zhang, H. S., Zhu, H., Peng, Y., Kang, L., Chen, J., and Park, S.-U.: Experiment on dust flux during dust storm period over sand desert area, *Acta Meteorological Sinica*, 65, 744–752, 2007.
- Zhang, X. Y., Arimoto, R., Zhu, G. H., Chen, T., and Zhang, G. Y.: Concentration, size-distribution and deposition of mineral aerosol over Chinese desert regions, *Tellus B*, 50, 317–330, 1998.

Zhao, H. L., Zhou, R. L., Su, Y. Z., Zhang, H., Zhao, L. Y., and Drake, S.: Shrub facilitation of desert land restoration in the Horqin Sand Land of Inner Mongolia, *Ecol. Eng.*, 31, 1–8, 2007.

5 Zhu, H. and Zhang, H. S.: Estimation of the threshold friction velocities over various dust storm source areas in northwest China, *Acta Meteorologica Sinica*, 548–557, 2010.

ACPD

13, 2671–2693, 2013

Size distributions of mineral aerosols and dust emission flux

X. Li and H. S. Zhang

Title Page

Abstract

Introduction

Conclusions

References

Tables

Figures

⏪

⏩

◀

▶

Back

Close

Full Screen / Esc

Printer-friendly Version

Interactive Discussion



Size distributions of mineral aerosols and dust emission flux

X. Li and H. S. Zhang

Table 1. Information of dust events observed in April 2012.

Date	Start Time (LT)	Duration	$DC_{\max,3m}$ ($\mu\text{g m}^{-3}$)	$U_{\max,4m}$ (m s^{-1})	WD ($^{\circ}$)
7 April	15:20–16:30	1 h 10 min	322.8	9.7	188–214
8 April	15:20–18:10	2 h 50 min	393.3	11.2	300–338
9 April	00:40–19:20	18 h 40 min	449.3	9.9	130–283
18 April	15:30–18:00	2 h 30 min	437.2	10.0	157–196
19 April	10:50–18:30	7 h 40 min	507.2	12.0	191–203
23–24 April	08:50–03:20	16 h 30 min	381.6	7.6	184–236
27 April	*–22:30	–	2324.9	13.4	285–308
29–30 April	16:50–02:00	9 h 10 min	302.7	8.4	189–213

* The beta gauges failed to measure the beginning period of the severe dust event because of the cutoff of electricity power.

Title Page

Abstract

Introduction

Conclusions

References

Tables

Figures

◀

▶

◀

▶

Back

Close

Full Screen / Esc

Printer-friendly Version

Interactive Discussion



Size distributions of mineral aerosols and dust emission flux

X. Li and H. S. Zhang

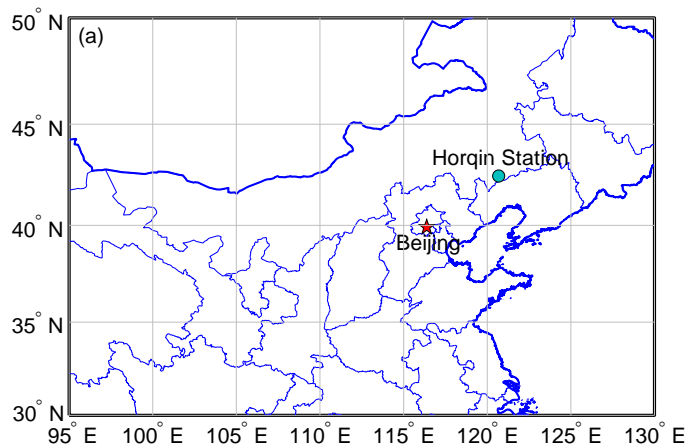


Fig. 1. (a) The location of the Naiman station, and (b) photo of the experiment site.

[Title Page](#)[Abstract](#)[Introduction](#)[Conclusions](#)[References](#)[Tables](#)[Figures](#)[◀](#)[▶](#)[◀](#)[▶](#)[Back](#)[Close](#)[Full Screen / Esc](#)[Printer-friendly Version](#)[Interactive Discussion](#)

Size distributions of mineral aerosols and dust emission flux

X. Li and H. S. Zhang

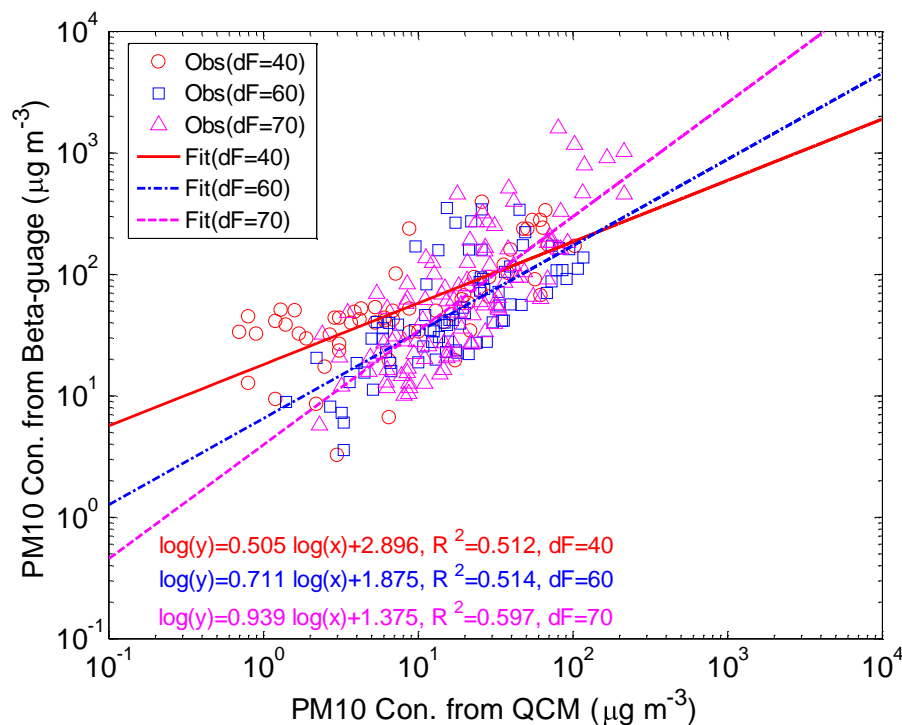


Fig. 2. Scatter plots of PM_{10} concentration measured by the QCM cascade impactor against that measured by beta gauge at the same time with the presetting frequency changes of 40 Hz (red circle), 60 Hz (blue square) and 70 Hz (magenta triangle). Optimal regression equations are given.

Title Page

Abstract

Introduction

Conclusions

References

Tables

Figures

◀

▶

◀

▶

Back

Close

Full Screen / Esc

Printer-friendly Version

Interactive Discussion



Size distributions of mineral aerosols and dust emission flux

X. Li and H. S. Zhang

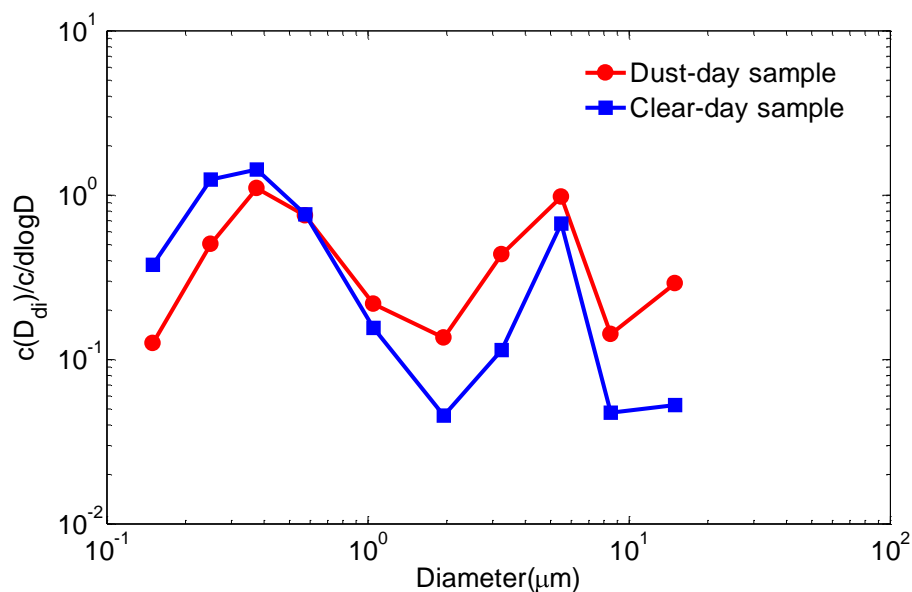


Fig. 3. Mean ratio of dust concentration of different sizes to the total PM₁₀ concentration measured by QCM cascade impactor under dust-day (solid line with red circle) and clear-day (solid line with blue square) conditions.

[Title Page](#)[Abstract](#)[Introduction](#)[Conclusions](#)[References](#)[Tables](#)[Figures](#)[◀](#)[▶](#)[◀](#)[▶](#)[Back](#)[Close](#)[Full Screen / Esc](#)[Printer-friendly Version](#)[Interactive Discussion](#)

Size distributions of mineral aerosols and dust emission flux

X. Li and H. S. Zhang

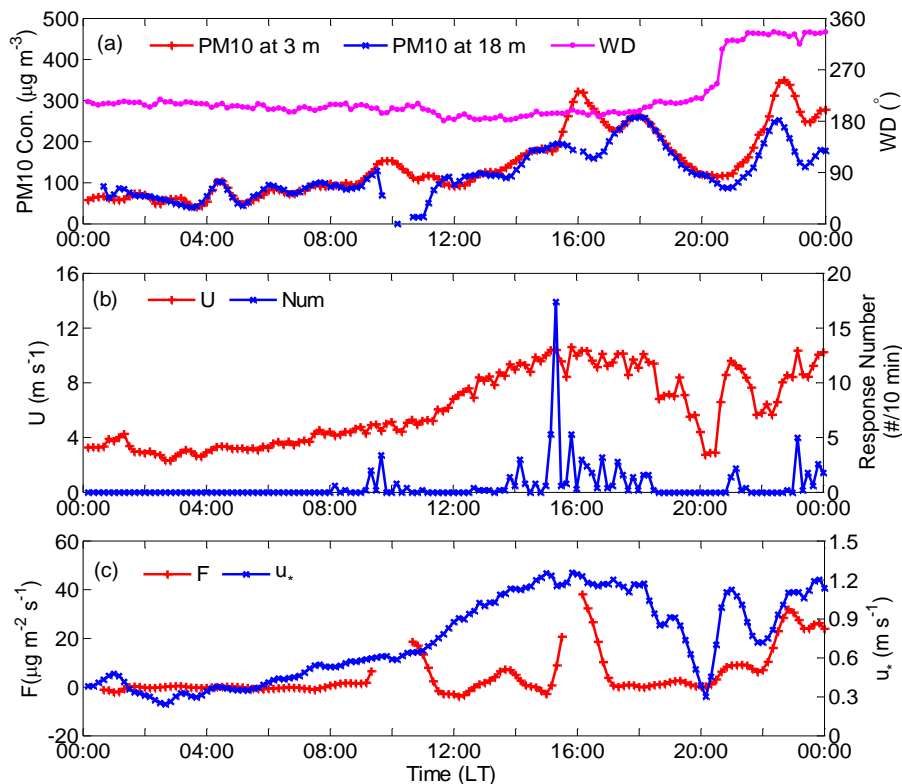


Fig. 4. Temporal variations of **(a)** dust (PM₁₀) concentration measured by beta gauge at 3 m and 18 m heights and wind direction, **(b)** 10-m wind speed and response number representing sand saltation intensity, and **(c)** dust emission flux F and friction velocity u_* during the dust event on 7 April 2012.

Title Page

Abstract

Introduction

Conclusions

References

Tables

Figures

◀

▶

◀

▶

Back

Close

Full Screen / Esc

Printer-friendly Version

Interactive Discussion



Size distributions of mineral aerosols and dust emission flux

X. Li and H. S. Zhang

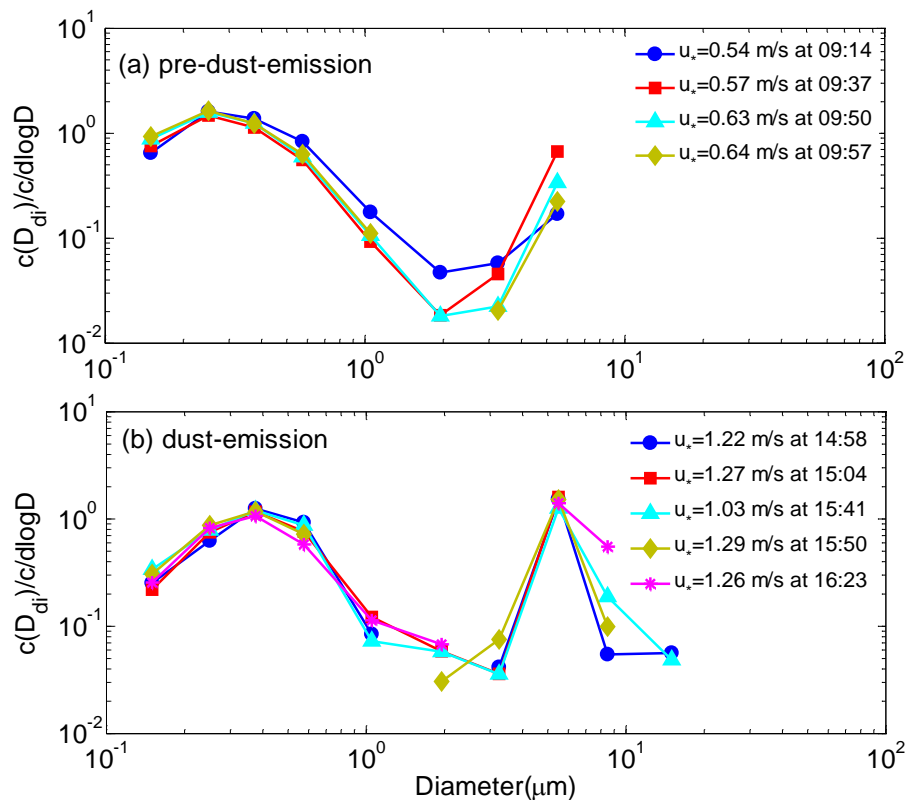


Fig. 5. Size distribution of airborne dust particles during **(a)** pre-dust-emissions and **(b)** dust-emission periods of the dust event on 7 April 2012.

[Title Page](#)
[Abstract](#)
[Introduction](#)
[Conclusions](#)
[References](#)
[Tables](#)
[Figures](#)
[◀](#)
[▶](#)
[◀](#)
[▶](#)
[Back](#)
[Close](#)
[Full Screen / Esc](#)
[Printer-friendly Version](#)
[Interactive Discussion](#)


Size distributions of mineral aerosols and dust emission flux

X. Li and H. S. Zhang

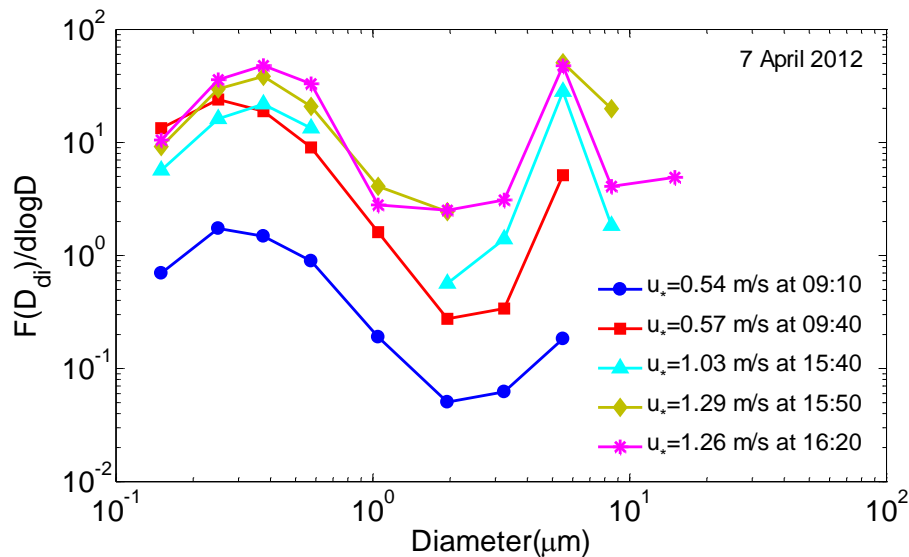


Fig. 6. Variations of size-resolved dust emission flux distributions under different friction velocity conditions during the dust event on 7 April 2012.

Title Page

Abstract

Introduction

Conclusions

References

Tables

Figures

◀

▶

◀

▶

Back

Close

Full Screen / Esc

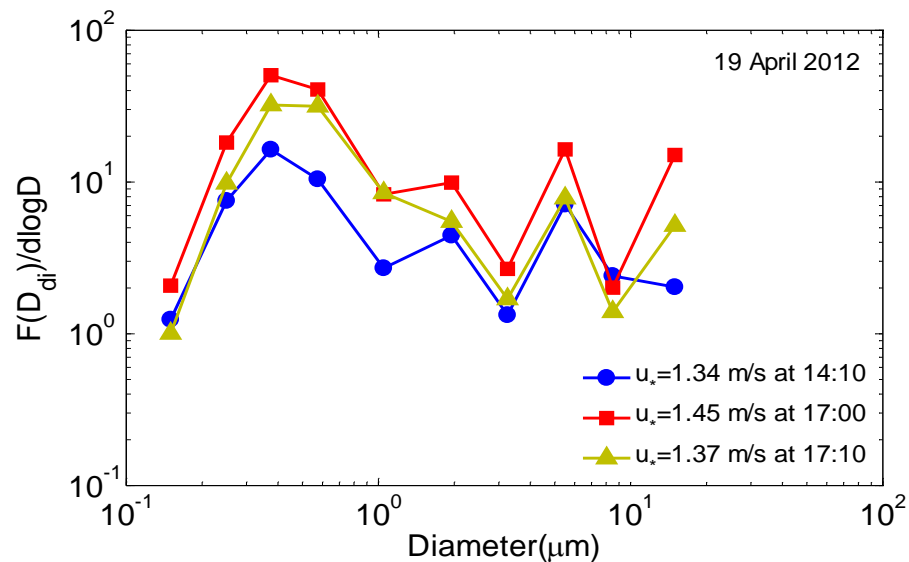
Printer-friendly Version

Interactive Discussion



Size distributions of mineral aerosols and dust emission flux

X. Li and H. S. Zhang

**Fig. 7.** Same as Fig. 6, but for 19 April 2012.

Title Page

Abstract

Introduction

Conclusions

References

Tables

Figures

◀

▶

◀

▶

Back

Close

Full Screen / Esc

Printer-friendly Version

Interactive Discussion



Size distributions of mineral aerosols and dust emission flux

X. Li and H. S. Zhang

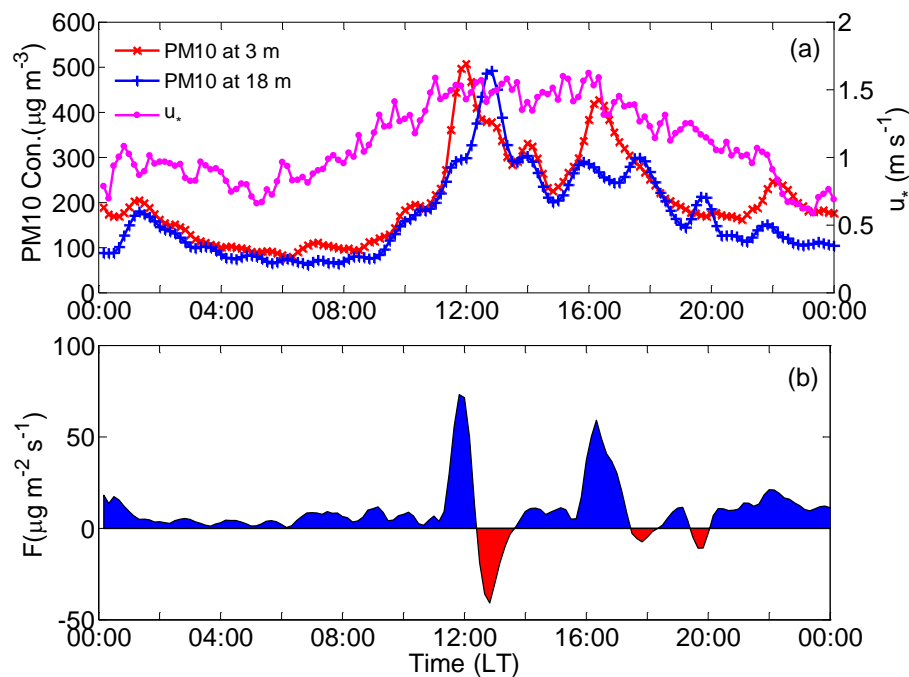


Fig. 8. Temporal variations of (a) PM_{10} concentration measured by beta gauge at 3 and 18 m height and friction velocity u_* , (b) dust emission flux F during the dust event on 19 April 2012.

Title Page

Abstract

Introduction

Conclusions

References

Tables

Figures

◀

▶

◀

▶

Back

Close

Full Screen / Esc

Printer-friendly Version

Interactive Discussion

